Dynamics of particle settling and resuspension in viscous liquids

N. Murisic[1] †, B. Pausader[2], D. Peschka[3], A.L. Bertozzi[1]

[1] Department of Mathematics, University of California, Los Angeles, 520 Portola Plaza, Los Angeles, California 90095, USA

[2] Courant Institute of Mathematical Sciences, New York University, 251 Mercer Street, New York , New York 10012, USA

[3] Weierstrass-Institute for Applied Analysis and Stochastics, Mohrenstr. 39, 10117 Berlin, Germany

(Received 7 February 2012)

We derive and study a dynamic model for suspensions of negatively buoyant particles on an incline. Our theoretical model includes the settling/sedimentation due to gravity as well as the resuspension of particles induced by shear-induced migration, leading to disaggregation of the dense sediment layer. Out of the three different regimes observed in the experiments, we focus on the so-called settled case, where the particles settle out of the flow, and two distinct fronts, liquid and particle, form. Using an approach relying on asymptotics, we systematically connect our dynamic model with the previously developed equilibrium theory for particle-laden flows. We show that the resulting transport equations for the liquid and the particles are of hyperbolic type, and study the dilute limit, for which we compute exact solutions. We also carry out a systematic experimental study of the settled regime, focusing on the motion of the liquid and the particle fronts. Finally, we carry out numerical simulations of our transport equations. We show that the model predictions for small to moderate values of the particle volume fraction and the inclination angle of the solid substrate agree well with the experimental data.

1. Introduction and Background

Despite their relevance to various industrial and environmental applications, the systems involving sedimentation, settling, and resuspension of particles in viscous liquids are still not fully understood. The seminal works on this subject, e.g. Kynch (1952); Richardson & Zaki (1954); Davis & Acrivos (1985); Schaflinger *et al.* (1990); Acrivos *et al.* (1992), have primarily focused on settling and sedimentation in quiescent liquid medium or in Couette flows. Our focus in this paper is on the particle-laden thin-film flows on an incline, involving a free surface and contact lines. Due to complexities resulting from a perplexing interplay of various relevant mechanisms, including settling/resuspension and viscous fingering at the contact line, only recent studies have began to address this class of problems, e.g. Zhou *et al.* (2005); Cook (2008). While particle-laden thin-film flows represent a formidable problem from the theoretical standpoint, these flows are captured through relatively simple experiments, see e.g. Ward *et al.* (2009); Murisic *et al.* (2011).

When a rigid spherically-shaped particle settles under the influence of gravity in a quiescent liquid, the well-known Stokes' Law applies. When a large number of such rigid spheres settles, the Stokes' Law is modified to include a hinderance term, accounting for

† Present address: Lewis-Sigler Institute for Integrative Genomics, Princeton University, Princeton, New Jersey 08544, USA

particle-particle interaction. This effect was first studied in Richardson & Zaki (1954), where a simple hinderance term $(1-\phi)^m$, with ϕ being the particle volume fraction and $m \approx 5.1$, was constructed empirically and included into expression for Stokes velocity as a multiplicative factor. Alternate forms of the hinderance function were proposed more recently, e.g. for dilute dispersions in Batchelor (1972), or $(1-\phi)$ in the presence of shear, see Schaflinger *et al.* (1990).

Experiments with concentrated suspensions in Couette flows showed that heavy particles need not settle when shear is present. This curious behavior was studied in detail in Leighton & Acrivos (1987*a*), and it was attributed to the so-called shear-induced migration mechanism, which was first formulated in Leighton & Acrivos (1987*b*) and then refined in Phillips *et al.* (1992). Shear-induced migration was derived based on irreversible interactions between pairs of particles. The particles migrate via a diffusive flux, induced by gradients in both the particle volume fraction, ϕ, and the suspension viscosity, $\mu(\phi)$. Subsequent works focused on particle-laden channel flows, and included shear-induced migration effect in the Stokesian Dynamics framework, see e.g. Nott & Brady (1994); Brady & Morris (1997); Timberlake & Morris (2005).

Only more recent works have focused on the problem of particle-laden thin-film flows on an incline. In Zhou *et al.* (2005), experiments were carried out using suspensions of glass beads with diameter $\sim \mathcal{O}(100\mu m)$. The bulk particle volume fraction, ϕ_0, and the inclination angle, α, were varied over a wide range, and it was found that, depending on the values of these two parameters, three different regimes occur. When ϕ_0 and α were small, the *settled* regime resulted, where the particles would settle out of the flow and the clear liquid would flow over the particulate bed. The two distinct fronts would form in this regime, a particle front and a clear liquid front. The former was found to be slower, and the latter was susceptible to the well-known fingering instability, typical for clear liquid films. For large values of ϕ_0 and α, the *ridged* regime occurred, where particles would flow faster than the liquid phase, and they would accumulate at the front of the flow, forming a ridge at the contact line. Finally, for intermediate values of ϕ_0 and α, the suspension would remain *well-mixed* throughout the experiment. The theoretical model developed in Zhou *et al.* (2005) was based on the Navier-Stokes equations for the liquid and a continuum diffusive model for the particles, including hindered settling. It was simplified by neglecting the capillary terms, and studied using a shock-dynamics approach, the direction further pursued in Cook *et al.* (2007). The model was successful at describing the details of the ridged regime. In order to better understand the three different regimes, the shear-induced migration was included for the first time in modeling of particle-laden thin-film flows in Cook (2008). In this work, an equilibrium model for particle settling was derived, based on the balance of hindered settling and shear-induced migration fluxes. The ODE-based model agreed well with the experimental data from Zhou *et al.* (2005). It captured the transitions from the well-mixed state and hinted at the transient nature of this regime. The work in Ward *et al.* (2009) was an experimental study of particle-laden thin-film flows on an incline, where the focus was on the front propagation in the well-mixed and ridged regimes, using both heavy and light particles. It was found that the front speed obeys a power law with an exponent close to the famous 1/3 from Huppert (1982). In Grunewald *et al.* (2010), the self-similarity in a lubrication-based model for the case of constant volume flows was explored. The main focus was on the ridged regime, and the influence of the precursor thickness on the model prediction was also studied. In Murisic *et al.* (2011), extensive experiments were carried out, where the influence of the particle size and the viscosity of the suspending liquid were examined. These experiments confirmed the transient nature of the well-mixed regime. An extension of the equilibrium model from Cook (2008) was employed, and a time-scales argument was introduced, explaining the dynamics of the transition between the well-mixed and settled regimes. Finally, a dynamic model for particle-laden thin film flows was introduced, based on a coupled set of hyperbolic conservation laws, and a connection between this model and the equilibrium one was indicated.

While, direct numerical simulations of the suspension flows coupled to many-particle-dynamics are possible nowadays, e.g. see Glowinski *et al.* (2001), these computations are usually limited a few thousand particles. Simulations of physically realistic situations are still far too computationally expensive when individual particles are considered. Therefore, the merit of using a continuum approach, in which one describes the evolution of statistical quantities such as particle volume fraction ϕ, volume averaged velocity $\mathbf{u}$, and pressure p is still quite apparent.

In this paper, our goal is to derive systematically a dynamic model for particle and liquid transport in order to better understand the less-studied settled regime. In order to achieve this aim, we carry out both theoretical and experimental work. We study a dense suspension flow on an incline, consisting of negatively buoyant particles with uniform size in a viscous suspending liquid. We concentrate on the *settled* regime, where gravity drives the flow down an incline, and leads to stratification of the suspension. We consider a continuum model, including the effects of hindered settling and shear-induced migration. The model is based on the Stokes' equations for an incompressible variable-viscosity suspension, and the conservation of total mass of particles. A dynamic model for transport of liquid and particles is developed in a systematic manner using an asymptotic approach. Due to the disparity in the relevant time-scales, a fast one for the settling and a slow one for the suspension flow, we are able to assume that the particle distribution is in equilibrium along the direction normal to the solid substrate (the settling direction) while the particles are transported along the solid substrate (the flow direction). Hence, we formally connect the equilibrium model with the dynamic one in a single framework. We study the derived dynamic model, explicitly confirm its hyperbolicity, and consider the dilute limit for which we derive the analytic solution. We also study the settled regime experimentally by carrying out extensive experiments where the bulk particle volume fraction and the inclination angle are varied over a wide range of values. In these experiments, we focus on the evolution of the two fronts, the particle and the liquid one. Finally, we solve the hyperbolic conservation laws numerically, and compare the model predictions with the experimental data.

This paper is organized as follows. In §2 we introduce the model and show how the lubrication approximation may be employed to find an advection equation for both the suspension volume and the particle volume fraction. Furthermore we explain how the details of this model depend on the bulk particle volume fraction and the inclination angle. This is followed by §3, where we introduce the experimental techniques and describe the experimental observations. Next, in §4, we solve the dynamic model numerically and compare the results with the experimental data. We conclude with a brief discussion.

2. Theory

We consider an inclined flow of a suspension consisting of a viscous liquid and spherical monodisperse non-colloidal negatively buoyant particles. The particles are assumed to be rigid and the liquid is incompressible. The modeling is carried out within the continuum limit. The flows are assumed to obey the transverse symmetry; therefore, the cross-section of the flow is considered throughout the paper. Henceforth, we use the subscripts p and ℓ to differentiate between quantities corresponding to the particles and the liquid respectively.

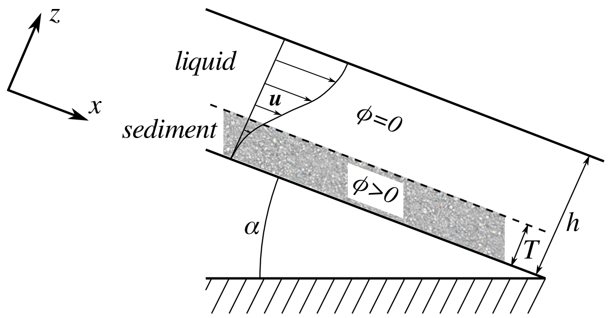

FIGURE 1. Sketch of a suspension flow with sediment layer.

Figure 1 shows the set-up (for clarity, the figure omits the contact line region). The x- and z-coordinates are in the directions along and normal to the solid substrate respectively. The solid substrate is located at $z = 0$ and the inclination angle of the solid is α. The total suspension thickness is denoted by $h(x,t)$. Our focus is on the *settled* regime for which a dense sedimentation layer of particles forms close to the solid substrate, the region $0 \le z \le T$ where $T < h$, with a clear liquid layer ($\phi = 0$) on top of it, $T < z \le h$. At each time t and point (x, z) the particle volume fraction, $0 \le \phi(t,x,z) < 1$, and the volume-averaged velocity, $\mathbf{u}(t,x,z) = (u(t,x,z), w(t,x,z))^\top$, are defined. For monodisperse spheres, the upper bound for ϕ is in fact less than unity: the maximum random packing volume fraction, $\phi_\mathrm{m} = 0.61$, was estimated experimentally in Murisic *et al.* (2011). We use this estimate as the upper bound for ϕ, and note that it lies between values 0.55 and 0.63 corresponding to random loose packing and random close packing respectively, see Song *et al.* (2008). Since the particles are heavy, the mass densities satisfy $\rho_p > \rho_\ell$. The suspension viscosity is assumed to depend on the particle volume fraction, i.e. $\mu = \mu(\phi)$. Finally, the incompressibility assumption translates to $\nabla \cdot \mathbf{u} = 0$.

In what follows, we derive a reduced model in which the local state can be uniquely characterized by average quantities. We also assume that the fastest dynamics is the instantaneous averaging of ϕ in the z-direction. As a result, the overall dynamics of the system is determined by a combination of two processes with very different time-scales: the fast process of ϕ averaging and the slow suspension flow down the incline. The fast process results in a stationarity of the particle fluxes in the z-direction, allowing us to reconstruct the ϕ and u dependence on z. In the slow process, h and u vary slowly in x, and the dynamics is driven by the conservation laws for the average quantities, e.g. the suspension volume and the number of particles.

2.1. *Two-phase model and lubrication equations*

For $\Omega_t = \{(x,z) : 0 < z < h(t,x)\}$, consider the following system of PDEs for the particle volume fraction $\phi : \Omega_t \to [0, \phi_\mathrm{m}]$ and the suspension velocity $\mathbf{u} : \Omega_t \to \mathbb{R}^2$

$$-\nabla \cdot \mathbf{\Pi} = \mathbf{f} \qquad (2.1a)$$

$$\partial_t \phi + \mathbf{u} \cdot \nabla \phi + \nabla \cdot \mathbf{J} = 0, \qquad (2.1b)$$

where $\mathbf{\Pi} = -p\mathbb{I} + \mu(\phi)(\nabla \mathbf{u} + \nabla \mathbf{u}^\top)$ is the stress tensor, the buoyancy is taken into account via $\mathbf{f} = (\rho_p \phi + \rho_\ell(1-\phi))\mathbf{g}$ and the acceleration of gravity is given by $\mathbf{g} = g(\sin\alpha, -\cos\alpha)^\top$. Henceforth, we utilize the notation for partial differentiation: $\partial_t[\cdot] = \frac{\partial}{\partial t}[\cdot]$ etc. The dependence of the suspension viscosity on ϕ is included through the so-called Krieger-Dougherty relation, $\mu(\phi) = \mu_\ell(1-\phi/\phi_\mathrm{m})^{-2}$, see Van Der Werff & De Kruif (1989) and Brady (1993). As written, Eqs. 2.1a) and b) are simply statements of the balance of linear momentum for the suspension (Stokes' equations) and the conservation of particle mass respectively. The particle fluxes are defined as in Murisic *et al.* (2011)

$$\mathbf{J} = \frac{d^2}{4}\left[K_c\begin{pmatrix}\partial_x(\dot\gamma\phi)\\ \partial_z(\dot\gamma\phi)\end{pmatrix} + \frac{2K_v\phi^2\dot\gamma}{\phi_{\rm m}-\phi}\begin{pmatrix}\partial_x\phi\\ \partial_z\phi\end{pmatrix}\right] - \frac{d^2(\rho_p-\rho_\ell)}{18\mu_\ell\phi_{\rm m}^2}\left[\phi(1-\phi)(\phi_{\rm m}-\phi)^2\mathbf{g}\right],$$

taking into account the shear-induced migration via the terms in the first brackets, see Phillips *et al.* (1992), and the hindered settling of particles due to gravity via the remaining term, as in Schaflinger *et al.* (1990). Here, K_c and K_v are empirical constants multiplying the contributions to the shear-induced particle flux due to gradients in the particle volume fraction and the effective suspension viscosity respectively; we follow Phillips *et al.* (1992) and use $K_c = 0.41$ and $K_v = 0.62$. The importance of including the shear-induced migration for successful description of the key feature of the suspension flow was shown previously in Cook (2008) and Murisic *et al.* (2011). We note that here, the hindrance to settling due to the wall-effect, used in Murisic *et al.* (2011), is neglected. The particle diameter is d, and the shear rate is given as usual, $\dot\gamma = \frac{1}{4}\|\nabla\mathbf{u}+\nabla\mathbf{u}^\top\|$. We also neglect the contribution to the particle flux due to Brownian motion, a reasonable approach since the relevant Péclet number is large, see Murisic *et al.* (2011).

Equations 2.1 are accompanied by the incompressibility condition, $\partial_x u + \partial_z w = 0$, and the following boundary conditions: no-slip and impermeability at the solid substrate, $u = w = 0$ at $z = 0$; the zero-shear-stress condition at the free surface, $\mathbf{t}\cdot\mathbf{\Pi n} = 0$ at $z = h$; and the zero-particle-flux conditions at both interfaces, $\mathbf{J}\cdot\mathbf{n} = 0$ at $z = 0$ and $z = h$; here, $\mathbf{n}$ is the outward-poining normal unit vector at the two interfaces, and $\mathbf{t}$ is the tangential unit vector at the free surface. The free surface evolves according to the kinematic condition, $\partial_t h = w - u\partial_x h$ at $z = h$.

Next, we scale Eqs. 2.1 in the spirit of the lubrication approximation, see e.g. Kondic & Bertozzi (1999), using the following scales

$$[x] = \varepsilon^{-1}H, \qquad [z] = H, \qquad [\phi] = 1,$$
$$[u] = \frac{H^2\rho_\ell g\sin\alpha}{\mu_\ell} = U, \qquad [w] = \varepsilon[u], \qquad [t] = [x]/[u],$$

where H is the typical thickness of the suspension film, while ε is the small lubrication-style parameter, to be defined shortly. Assuming that the settling and the suspension velocities are not modified by the hinderance, the typical distance a particle travels in the x-direction as it settles down to the solid substrate is given as a product of the relevant time- and velocity-scales

$$\frac{H/\cos\alpha}{U_{\rm St}}U = H\eta^{-2}\frac{18}{\rho_s}\tan\alpha, \tag{2.2}$$

where $\rho_s = (\rho_p-\rho_\ell)/\rho_\ell$, $\eta = d/H$, and the Stokes settling velocity of a single particle is given as $U_{\rm St} = gd^2(\rho_p-\rho_\ell)/(18\mu_\ell)$. Clearly, when $\eta\to 1$, the continuum hypothesis breaks down. On the other hand, for $\eta\to 0$, the transport of the particles is purely convective, the settling time-scale goes to infinity, and the suspension behaves like a colloid. Here, we want to derive a continuum model where the particle flux in the z-direction is in equilibrium. Therefore, we first require that $\eta^2 \ll 1$. In order for the equilibrium assumption to hold, it is also necessary to assume that the typical travel distance defined by Eq. 2.2 is asymptotically smaller than the lubrication length scale, $[x] = H/\varepsilon$. Hence, we need to consider

$$\varepsilon \ll \eta^2 \ll 1. \tag{2.3}$$

One way to achieve this is to set $\eta^2 = \varepsilon^\beta$ where $0 < \beta < 1$. Applying the scales to

Eq. 2.1b), while keeping in mind the definition of η, gives

$$\begin{aligned}\partial_t\phi + u\partial_x\phi + w\partial_z\phi = \ & \varepsilon^\beta \frac{K_c}{4}\left[\varepsilon\partial_x\left(\phi\partial_x(\dot\gamma\phi)\right) + \varepsilon^{-1}\partial_z\left(\phi\partial_z(\dot\gamma\phi)\right)\right] \\ & +\varepsilon^\beta\frac{K_v}{2}\left[\varepsilon\partial_x\left(\frac{\phi^2\dot\gamma}{\phi_{\mathrm{m}}-\phi}\partial_x\phi\right) + \varepsilon^{-1}\partial_z\left(\frac{\phi^2\dot\gamma}{\phi_{\mathrm{m}}-\phi}\partial_z\phi\right)\right] \\ & -\varepsilon^\beta\frac{\rho_s}{18\phi_{\mathrm{m}}^2}\left[\partial_x\left(\phi(1-\phi)(\phi_{\mathrm{m}}-\phi)^2\right)\right] \\ & +\varepsilon^\beta\frac{\rho_s\cot\alpha}{18\phi_{\mathrm{m}}^2}\left[\varepsilon^{-1}\partial_z\left(\phi(1-\phi)(\phi_{\mathrm{m}}-\phi)^2\right)\right]. \end{aligned} \tag{2.4}$$

We proceed by defining the asymptotic expansions of the solution

$$\begin{aligned}\phi(t,x,z) &= \phi^0(t,x,z) + o(1) \\ u(t,x,z) &= u^0(t,x,z) + o(1) \\ w(t,x,z) &= \varepsilon w^0(t,x,z) + o(\varepsilon) \\ h(t,x) &= h^0(t,x) + o(1).\end{aligned}$$

This also sets the expansions for the particle flux, $\mathbf{J} = \varepsilon^{\beta-1}\left(J_x^*, J_z^0 + J_z^*\right)^\top$, and for the shear rate, $\dot\gamma = \partial_z u^0 + o(1)$. Here, J_z^0 is $\mathcal{O}(1)$, and the higher order flux corrections are $J_x^* = o(\varepsilon)$ and $J_z^* = o(1)$, the subscripts denoting the directions in which they act. Using these expansions in Eq. 2.4 leads to

$$\begin{aligned}\partial_t\phi^0 + u^0\partial_x\phi^0 + w^0\partial_z\phi^0 = \varepsilon^{\beta-1}\partial_z J_z^0 + \varepsilon^{\beta-1}\partial_z J_z^* + o(\varepsilon^\beta) = \\ \varepsilon^{\beta-1}\partial_z\Bigg[\frac{K_c}{4}\phi^0\partial_z(\phi^0\partial_z u^0) + \frac{K_v}{2}\frac{(\phi^0)^2\partial_z u^0}{\phi_{\mathrm{m}}-\phi^0}\partial_z\phi^0 \\ +\frac{\rho_s\cot\alpha}{18}\phi^0(1-\phi^0)\left(\frac{\phi_{\mathrm{m}}-\phi^0}{\phi_{\mathrm{m}}}\right)^2\Bigg] + \varepsilon^{\beta-1}\partial_z J_z^* + o(\varepsilon^\beta).\end{aligned} \tag{2.5}$$

The leading order terms are $\mathcal{O}(\varepsilon^{\beta-1})$, describing the effect of the most dominant particle flux, J_z^0. We drop the "0" superscript for simplicity, and integrate the leading order terms in Eq. 2.5 with respect to z, while using either of the zero-flux boundary conditions. This results in

$$0 = \frac{K_c}{4}\phi(u'\phi)' + \frac{K_v}{2}\frac{\phi^2 u'\phi'}{\phi_{\mathrm{m}}-\phi} + \frac{\rho_s\cot\alpha}{18}\phi(1-\phi)\left(\frac{\phi_{\mathrm{m}}-\phi}{\phi_{\mathrm{m}}}\right)^2, \tag{2.6}$$

where primes indicate differentiation with respect to z. This equation is complemented by the zero-flux boundary conditions, $J_z(0) = J_z(h) = 0$, one of which has already been used in the previous integration. Using a similar approach on Eq. 2.1a) leads to

$$\left(\mu(\phi)u'\right)' = -(1+\rho_s\phi), \tag{2.7}$$

where $\mu(\phi) = (1-\phi/\phi_{\mathrm{m}})^{-2}$, accompanied by the no-slip and zero-shear-stress boundary conditions, $u = 0$ at $z = 0$, and $\mu(\phi)u' = 0$ at $z = h$ respectively.

The system of ODEs given by Eqs. 2.6 and 2.7 is very similar to the ones previously derived in Cook (2008) and Murisic *et al.* (2011): it constitutes the equilibrium model for the particle settling. This model has a one-parameter family of solutions, which may be parameterized by the integrated volume fraction of particles, defined as

$$n(t,x) = \int_0^h \phi(t,x,z)\,\mathrm{d}z. \tag{2.8}$$

In other words, once n is fixed, the z-dependence of ϕ and u may be determined uniquely from Eqs. 2.6 and 2.7, and the accompanying boundary conditions. In order to indicate that the dependence on z at the leading order solution is only parametrical through n, we write $\phi = \phi(t,x;z)$ and $u = u(t,x;z)$. We note that the initial values $n(0,x)$ may be obtained using the initial data, but the time-dependence of n is still unknown at this point. In order to determine this time-dependence, we are required to proceed to the next-order correction in Eq. 2.5, i.e. the $\mathcal{O}(1)$ terms. We practice caution by also maintaining the higher order correction term to the particle flux, J_z^*, and obtain

$$\partial_t \phi + u\partial_x \phi + w\partial_z \phi = \varepsilon^{\beta-1}\partial_z J_z^*. \tag{2.9}$$

To close the system and cast the dynamic model into a concrete framework together with the equilibrium model from Eqs. 2.6 and 2.7, we integrate Eq. 2.9 in the z-direction, from $z = 0$ to $z = h$. The flux correction term drops out via the use of the zero-flux boundary conditions. Using $\partial_t \int_0^h \phi dz = \phi \partial_t h|_{z=h} + \int_0^h \partial_t \phi dz$, and the kinematic condition, $\partial_t h = w - u\partial_x h$ at $z = h$, gives

$$\partial_t \int_0^h \phi dz = \phi(w - u\partial_x h)|_{z=h} - \int_0^h u\partial_x \phi dz - \int_0^h w\partial_z \phi dz.$$

Here, the first integral on the right-hand side is evaluated using the chain rule and the fact that $\partial_x \int_0^h \phi u dz = \phi u \partial_x h|_{z=h} + \int_0^h \partial_x (\phi u)\, dz$; the second integral on the right-hand side is integrated by parts. We then employ the impermeability condition, $w|_{z=0} = 0$, and the incompressibility condition, $\partial_x u + \partial_z w = 0$, to obtain

$$\partial_t \int_0^h \phi dz + \partial_x \int_0^h \phi u dz = 0.$$

Finally, recalling the definition of n gives

$$\partial_t n + \partial_x \int_0^h \phi(t,x;z)u(t,x;z)\, \mathrm{d}z = 0, \tag{2.10a}$$

an advection equation for the particle number n. This is a conservation law for the particles.

The corresponding advection equation for the suspension volume is obtained by first substituting $\partial_x \int_0^h u dz = u\partial_x h|_{z=h} + \int_0^h \partial_x u dz$ into the kinematic condition to get

$$\partial_t h + \partial_x \int_0^h u dz = w|_{z=h} + \int_0^h \partial_x u dz.$$

Here, the terms on the right-hand side add to zero: this can be seen by evaluating the integral on the right-hand side, and using incompressibility, $\partial_x u = -\partial_z w$, and impermeability, $w|_{z=0} = 0$. Hence, we obtain

$$\partial_t h + \partial_x \int_0^h u(t,x;z)\, \mathrm{d}z = 0, \tag{2.10b}$$

a conservation law for the suspension volume. Finally, it is convenient to rewrite the equilibrium equations in terms of the stress $\sigma = \mu(\phi)u'$

$$\frac{K_c}{4}\phi\left(\frac{\phi\sigma}{\mu(\phi)}\right)' + \frac{K_v}{2}\frac{\sigma\phi'}{\mu(\phi)}\frac{\phi}{\phi_{\mathrm{m}} - \phi} + \frac{\rho_s \cot\alpha}{18}\frac{\phi(1-\phi)}{\mu(\phi)} = 0 \tag{2.10c}$$

$$\sigma' = -(1 + \rho_s \phi), \tag{2.10d}$$

with the boundary conditions $u(0) = 0$, $J_z(0) = J_z(h) = 0$, and $\sigma(h) = 0$. Equations 2.10

give the full theoretical framework. We note that conservation laws similar to Eqs. 2.10a) and b) were introduced in Murisic *et al.* (2011), but without any formal derivation. While they were expected to be hyperbolic, it was found that the loss of hyperbolicity seemed to occur for certain parameter values, well within the physically meaningful range. We will address the topic of hyperbolicity below.

2.2. *Particle transport model and fluxes*

Equations 2.10 may be simplified by eliminating the explicit h dependence from the equilibrium model. We carry this out by scaling z with h: $s = z/h$. Equations 2.10 are then rewritten using $\phi(t,x;z) = \phi(t,x;h(t,x)s) = \tilde{\phi}(t,x;s)$, $u(t,x;z) = u(t,x;h(t,x)s) = h(t,x)^2\tilde{u}(t,x;s)$, and $\tilde{\sigma}(t,x;s) = \sigma(t,x;h(t,x)s)/h(t,x) = \mu(\tilde{\phi}(t,x;s))\tilde{u}'(t,x;s)$; henceforth, the prime denotes the differentiation with respect to s. The result is

$$\partial_t h + \partial_x F(h,n) = 0 \tag{2.11a}$$

$$\partial_t n + \partial_x G(h,n) = 0, \tag{2.11b}$$

where the suspension and particle fluxes, F and G respectively, are written in terms of $\tilde{\phi}$ and $\tilde{u}$

$$F(h,n) = \int_0^h u(t,x;z)\mathrm{d}z = h^3\int_0^1 \tilde{u}(t,x;s)\,\mathrm{d}s = h^3 f(\phi_0) \tag{2.11c}$$

$$G(h,n) = \int_0^h \phi(t,x;z)u(t,x;z)\mathrm{d}z = h^3\int_0^1 \tilde{\phi}(t,x;s)\tilde{u}(t,x;s)\,\mathrm{d}s = h^3 g(\phi_0). \tag{2.11d}$$

It is also convenient to introduce the z-averaged particle volume fraction

$$\phi_0(t,x) = \int_0^1 \tilde{\phi}(t,x;s)\,\mathrm{d}s = \frac{n(t,x)}{h(t,x)} \in [0,\phi_{\mathrm{m}}]. \tag{2.11e}$$

Next, the equilibrium equations are rewritten as

$$\left(1 + C_1\frac{\tilde{\phi}}{\phi_{\mathrm{m}} - \tilde{\phi}}\right)\tilde{\sigma}\tilde{\phi}' + C_2 - (C_2+1)\tilde{\phi} - \rho_s\tilde{\phi}^2 = 0, \tag{2.11f}$$

$$\tilde{\sigma}' = -(1+\rho_s\tilde{\phi}), \tag{2.11g}$$

for $0 \le s \le 1$, with the boundary condition $\tilde{\sigma}(1) = 0$; here,

$$C_1 = \frac{2(K_v - K_c)}{K_c}, \qquad C_2 = \frac{2\rho_s \cot\alpha}{9K_c}.$$

The equilibrium model, Eqs. 2.11f) and g), is solved for the intermediate variables $\tilde{\sigma}$ and $\tilde{\phi}$; $\tilde{u}$ is recovered from $\tilde{\sigma} = \mu(\tilde{\phi})\tilde{u}'$ using the no-slip boundary condition at $s = 0$. These profiles are then supplied to the transport equations, Eqs. 2.11a-e), to close the system: the suspension and the particle fluxes are determined by the functions f and g of a single real argument, which is found by solving Eqs. 2.11f) and g) for $s \in [0,1]$ and a given value of ϕ_0. We note that the cubic dependence of the fluxes F and G on h, reminiscent of factors appearing in the thin film equation, e.g. see Kondic (2003), results from the exact scaling invariance of the leading order ODEs, Eqs. 2.10c) and d).

For a given value of ϕ_0, the solution to the system 2.11 is unique. Within this one-parameter family, two distinct types of solutions exist. The first type occurs for smaller ϕ_0 values and it is characterized by monotonically decreasing profiles for $\tilde{\phi}$. In particular, with $0 < \tilde{T} = T/h < 1$, the resulting $\tilde{\phi}(s)$ is strictly decreasing for $0 \le s \le \tilde{T}$, leading to $\tilde{\phi}(\tilde{T}) = 0$; the solution is then continued with $\tilde{\phi}(s) = 0$ for $\tilde{T} < s < 1$. The second type

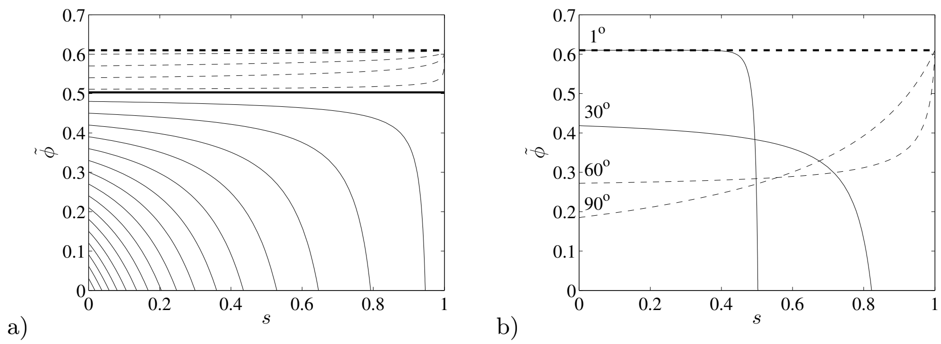

FIGURE 2. Particle volume fraction profiles $\widetilde{\phi}(s)$ for different values of α and ϕ_0, resulting in *settled* (solid lines) and *ridged* regimes (dashed lines): a) fixed $\alpha = 25^\circ$ and various average concentrations ϕ_0, increasing in steps of 0.028 from 0 to $\phi_{\rm m}$ (heavy dashed line) via $\widetilde{\phi}_{crit} = 0.476$ (heavy solid line); b) fixed $\phi_0 = 0.3$ and different inclination angles $\alpha = (1, 30, 60, 90)^\circ$.

of solutions occurs for larger values of ϕ_0 and it is characterized by strictly increasing $\tilde{\phi}(s)$ profiles, where $\tilde{\phi}(s) \to \phi_{\rm m}$ as $s \to 1$. Here, the focus is solely on the first type of solutions, since it corresponds to the settled regime, which is expected for small values of α and ϕ_0. The second type of solutions corresponds to the ridged regime. The critical concentration, $\tilde{\phi}_{crit}$, separating the two extreme regimes, is determined by the constant-concentration solution, i.e. setting $\tilde{\phi}' = 0$ in 2.11f), and solving for the average particle volume fraction

$$\tilde{\phi}_{crit} = \min\left\{\phi_{\rm m}, \frac{-(C_2+1)}{2\rho_s} + \sqrt{\left(\frac{C_2+1}{2\rho_s}\right)^2 + \frac{C_2}{\rho_s}}\right\}. \tag{2.12}$$

This defines the unstable well-mixed state. Figure 2 shows the two families of solutions for $\tilde{\phi}$, including the well-mixed state occurring for $\tilde{\phi}_{crit}$. The solutions are obtained numerically, using a shooting method, see Murisic *et al.* (2011).

2.3. *Dilute approximation*

For small particle concentrations, i.e. $\phi, \tilde{\phi} \ll 1$, we are able to compute the fluxes analytically. In this limit, the hyperbolicity of the conservation laws may also be confirmed explicitly. Assuming $\phi_0, \tilde{\phi}(s) \ll \phi_{\rm m}$, we linearize Eqs. 2.11f) and g) with respect to $\tilde{\phi}$, and, to the leading order, obtain

$$\tilde{\sigma}\tilde{\phi}' = -C_2 \qquad\qquad 0 \le s \le \tilde{T} \tag{2.13}$$

$$\tilde{\sigma}' = -1 \qquad\qquad 0 \le s \le 1, \tag{2.14}$$

with $\tilde{\sigma}(1) = 0$. To the leading order in $\tilde{\phi}$, the solution to this system of ODEs is

$$\tilde{\sigma}(s) = 1 - s \tag{2.15}$$

$$\tilde{\phi}(s) = \begin{cases} C_2(\tilde{T} - s) & 0 < s \le \tilde{T} \\ 0 & \tilde{T} < s \le 1, \end{cases} \tag{2.16}$$

resulting in the average concentration

$$\phi_0 = \int_0^1 \tilde{\phi}(s)\,\mathrm{d}s = \frac{C_2\tilde{T}^2}{2}. \tag{2.17}$$

By using $\tilde{\sigma} = \mu(\tilde{\phi})\tilde{u}' \approx \mu(0)\tilde{u}'$, we are also able to find the velocity $\tilde{u}(s)$ to the leading order

$$\tilde{u}(s) = \int_0^s \frac{\tilde{\sigma}(r)}{\mu(\tilde{\phi}(r))}\,\mathrm{d}r = \int_0^s \frac{(1-r)}{\mu(0)}\left(1+\mathcal{O}(\tilde{\phi})\right)\,\mathrm{d}r = \left(s - \frac{s^2}{2}\right) + \mathcal{O}(\tilde{\phi}).$$

Therefore, the use of (2.17) leads to the leading order for the particle flux

$$\begin{aligned} g(\phi_0) &= \int_0^1 \tilde{\phi}(s)\tilde{u}(s)\,\mathrm{d}s = \int_0^{\tilde{T}} C_2(\tilde{T}-s)\left(s-\frac{s^2}{2}\right)\,\mathrm{d}s \\ &= C_2\left(\frac{\tilde{T}^3}{6} - \frac{\tilde{T}^4}{24}\right) = \sqrt{\frac{2}{9C_2}}\phi_0^{3/2} + \mathcal{O}(\phi_0^2). \end{aligned}$$

Also, the leading order for the suspension volume flux is

$$f(\phi_0) = \int_0^1 \tilde{u}(s)\,\mathrm{d}s = \frac{1}{3}.$$

Finally, to the leading order, the hyperbolic transport laws in the dilute limit are given by

$$\partial_t h + \partial_x\left(\frac{h^3}{3}\right) = 0, \tag{2.18a}$$

$$\partial_t n + \partial_x\left(\sqrt{\frac{2}{9C_2}}(nh)^{3/2}\right) = 0. \tag{2.18b}$$

Here, we make a note regarding the apparent loss of hyperbolicity for the conservation laws discussed in Murisic *et al.* (2011). In particular, in Murisic *et al.* (2011), the suspension and particle fluxes appearing in the conservation laws were fitted from the solutions of the equilibrium problem via the least-squares polynomials in h and ϕ_0, i.e. using only integer powers of h and ϕ_0. Equations 2.18 indicate that such an approach is rather problematic, since, at least in the dilute limit, fractional powers in h and ϕ_0 are required in order to accurately capture the behavior of the fluxes. Hence, the loss of hyperbolicity discussed in Murisic *et al.* (2011) was likely caused by the ill-suited fitting approach rather than the mathematical structure of the conservation laws – their inherent hyperbolicity is confirmed below.

We proceed by solving Eqs. 2.18 exactly for the fixed suspension volume case, with the initial data $h(0,x) = \chi\{0 \le x \le 1\}$, $n(0,x) = f_0 h(0,x)$, and some given value of $f_0 \ll 1$. Since ϕ_0 is small in the dilute limit, we abbreviate $\xi = 1/\sqrt{2C_2}$ and solve Eq. 2.18a) for h independently to get

$$h(t,x) = \begin{cases} 1 & t \le x \le x_\ell(t) \\ \sqrt{x/t} & 0 < x < \min\big(t, x_\ell(t)\big) \\ 0 & \text{else,} \end{cases} \tag{2.19}$$

for $t \ge 0$, where the liquid front position is

$$x_\ell(t) = \begin{cases} 1 + t/3 & 0 \le t \le 2/3 \\ \left(\frac{9t}{4}\right)^{1/3} & 2/3 < t. \end{cases}$$

This is the well-known solution computed by Huppert (1982). Next, we may use this solution to find the solution for n as follows. First note that for early times, the solution for n also consists of a rarefaction fan for $0 < x < t$, connected to a constant with value

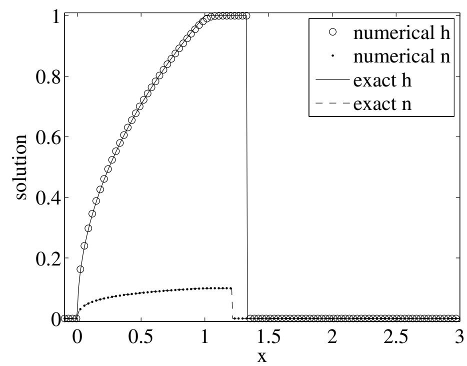

FIGURE 3. Exact vs. numerical solution in the dilute limit at $t = 1$ for $\xi = 1$ and $f_0 = 0.1$

f_0 in $t \leq x \leq 1 + \xi f_0^{1/2} t$. For larger values of x, the integrated particle volume fraction n vanishes. The evolution equation for n may be written as

$$\partial_t n + \frac{2\xi}{3} \partial_x \big(h(t,x)n(t,x)\big)^{3/2} = 0. \tag{2.20}$$

Note that by the assumption of dilute regime, we always have $x_p < x_\ell$. Clearly, the problem amounts to determining the shape of the rarefaction fan for n. To resolve it, we assume thet $n(t,x) = N(\omega)$, where $\omega = x/t$ is a rarefaction fan starting at zero, i.e. $\omega > 0$. Substituting this ansatz into Eq. 2.20 gives the following ODE for N

$$-2\omega^{5/4} N'(\omega) + \xi \sqrt{N(\omega)} \big[N(\omega) + 2\omega N'(\omega)\big] = 0. \tag{2.21}$$

The solution is

$$N(\omega) = \xi^{-1} \left(c - 2\sqrt{\frac{c^4\xi^2 + c^3\xi\sqrt{\omega}}{\omega}} \right) + \frac{2c^2}{\sqrt{\omega}}, \tag{2.22}$$

where c is an undetermined constant of integration. We note that this solution satisfies $N(\omega) \to 0$ as $\omega \to 0$. For our purposes, we may fix c by requiring that the continuity is obeyed, i.e. that $n(t,t) = N(1) = f_0$, which results in $c = f_0\xi/(1 - 2\xi\sqrt{f_0})$. Finally, this gives us our solution

$$n(t,x) = \begin{cases} f_0 & t \leq x \leq x_p(t) \\ N(x/t) & 0 < x < \min\big(t, x_p(t)\big) \\ 0 & \text{else,} \end{cases} \tag{2.23}$$

and the particle front position is $x_p(t) = \min(1 + \frac{2\xi}{3} f_0^{1/2} t, \bar{x}_p(t))$, where $\bar{x}_p$ satisfies

$$\int_0^{\bar{x}_p/t} N(x/t)\,\mathrm{d}x = f_0. \tag{2.24}$$

Using $\bar{x}_p/t \to 0$ as $t \to \infty$, and $N(\omega) = \sqrt{\omega}/(4\xi^2) + O(\omega)$ we get $\bar{x}_p(t) = 6^{1/3}(\xi^4 f_0^2 t)^{1/3}$. Hence,

$$\lim_{t\to\infty} \frac{x_p(t)}{x_\ell(t)} = \left(\frac{24\xi^4 f_0^2}{9}\right)^{1/3}.$$

We note that the value of this limit is independent of the choice of the integration constant c appearing in the solution of the rarefaction-fan. Furthermore, $N(\omega)$ calculated in Eq. 2.22 is the generic candidate for describing the long-time evolution of the particle

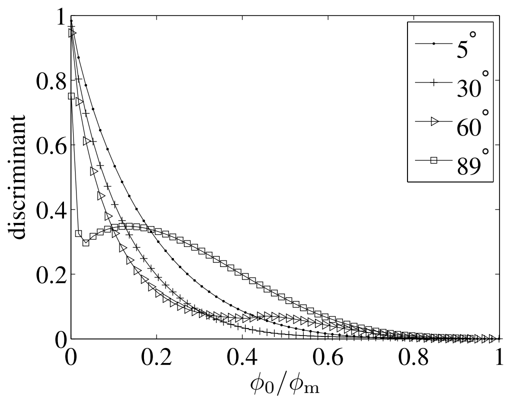

FIGURE 4. Discriminant D vs. ϕ_0/ϕ_m for inclination angles $\alpha = (5, 30, 60, 89)^\circ$.

distribution. In particular, while $N(\omega)$ is determined by the mechanisms responsible for fixing the value of the integration constant c during the early transient time-intervals, its expansion as $\omega \to 0$, i.e. as $t \to \infty$, is independent of c. Equations 2.18 may also be solved numerically using an upwind scheme. Figure 3 shows that the exact and the numerical solutions of Eqs. 2.18 coincide.

Next, we study the hyperbolicity of Eqs. 2.11a) and b), and the parameter dependence of the suspension and particle volume fluxes, f and g respectively, by solving Eqs. 2.11f) and g) numerically for $\tilde{\phi}(s)$ and $\tilde{\sigma}(s)$.

2.4. *Hyperbolicity*

The transport problem reads

$$\partial_t h + \partial_x\left(h^3 f(\tfrac{n}{h})\right) = 0 \tag{2.25}$$

$$\partial_t n + \partial_x\left(h^3 g(\tfrac{n}{h})\right) = 0, \tag{2.26}$$

after opting for f and g rather than F and G, and using the definitions in Eqs. 2.11c) and d). The Jacobian associated with the above system of conservations laws is

$$J = h^2 \begin{pmatrix} 3f - \phi_0 f' & f' \\ 3g - \phi_0 g' & g' \end{pmatrix},$$

and the discriminant of the corresponding characteristic polynomial is

$$D = h^4[(g' + \phi_0 f' - 3f)^2 + 4f'(3g - \phi_0 g')].$$

Here, the primes denote differentiation with respect to ϕ_0. The hyperbolicity of the transport problem is ensured when $D \geq 0$. We note that the Jacobian and the discriminant are obtained using the intermediate variable $n = \phi_0 h$, where the Jacobian is derived in terms of the (h, n) problem, and then rewritten again in terms of h and ϕ_0. This is rather convenient because h may be scaled out of the discriminant, and what remains is a condition for hyperbolicity on $f(\phi_0)$, $g(\phi_0)$, and their derivatives with respect to ϕ_0. Figure 4 shows that the discriminant remains strictly positive for all ϕ_0 values within physically meaningful range, $\phi_0 \in [0, \phi_\mathrm{m}]$, and all tested values of the inclination angle. Therefore, we conclude that our system of conservation laws, Eqs. 2.11a) and b), is a well-posed hyperbolic problem for the variables h and n.

We proceed by studying the suspension and particle volume fluxes, f and g respectively, for various parameter values, by solving Eqs. 2.11f) and g) numerically for $\tilde{\phi}(s)$ and

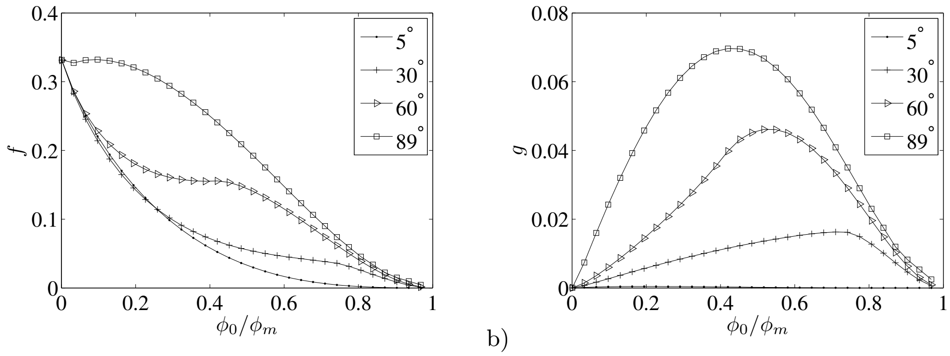

a) b)

FIGURE 5. Fluxes f in a), and g in b) for inclination angles $\alpha = (5, 30, 60, 89)^\circ$.

$\tilde{\sigma}(s)$. Fluxes f and g for various values of the inclination angle α are shown in Fig. 5. For small values of α, the suspension volume flux f decreases as ϕ_0 increases due to a corresponding increase in the effective suspension viscosity. Only for large values of α, the flux f increases with ϕ_0, due to to the increase in the corresponding suspension mass and gravitational shear force. For $\phi_0 \to 0$, one recovers the standard lubrication flux, $F = h^3/(3\mu_l)$, while for $\phi_0 \to \phi_{\mathrm{m}}$, the suspension flux tends to zero, $F \to 0$, due to the fact that $\mu \to \infty$. The particle volume flux g increases with ϕ_0, due to the increase in the particle content. However, the increase is sublinear since increasing ϕ_0 causes a decrease in the flow velocity, u, as already observed for flux f. Therefore, g must be zero at both $\phi_0 = 0$ and $\phi_0 = \phi_{\mathrm{m}}$, as evidenced by Fig. 5.

The transition from the settled regime to the ridged regime occurs when the average particle velocity exceeds the average suspension velocity, i.e. when $g/\phi_0 \geq f$ or equivalently, when

$$\frac{\int_0^1 \tilde{\phi}\tilde{u}\, ds}{\int_0^1 \tilde{\phi}\, ds} \geq \int_0^1 \tilde{u}\, ds.$$

With $\tilde{u}$ being an increasing positive function and $\tilde{\phi} > 0$, this transition occurs when $\tilde{\phi}$ changes monotonicity, which happens at the value $\tilde{\phi}_{crit}$ given by Eq. 2.12.

3. Experiments

We carry out experiments with gravity driven particle-laden thin films using an inclined solid setup. A thorough description of this apparatus was included in Murisic *et al.* (2011); we only list the main specifications here.

The apparatus consists of an acrylic track, $90cm$ long, $14cm$ wide, with $1.5cm$-tall side walls. A gated reservoir with acrylic walls is situated at the top of the track; its interior is $14cm$ wide and $10cm$ long; the release gate is manually operated. The collecting tank is at the bottom of the track. The typical thickness of the particle-laden thin film in our experiments is $H \sim 1cm$. The inclination angle of the track, α, may be manually adjusted in the range $5-80^\circ$ with precision within a few percent. The suspending liquid we use is PDMS (AlfaAesar) with the kinematic viscosity $\nu_\ell = 1000\, cSt$ and density $\rho_\ell = 971\, kg\, m^{-3}$. The particles are smooth spherical glass beads (Ceroglass) with diameter $d = 337\mu m$ (standard deviation $\approx 26\%$) and density $\rho_p = 2475\, kg\, m^{-3}$. The decision to use this particular particle size is influenced by the need to fulfill the requirement $\varepsilon \ll \eta^2 \ll 1$, derived in §2; the other available sizes either fail in this task (smaller particles), or make the continuum assumption questionable (large ones).

We focus on the constant suspension volume experiments: each experimental run is carried out using $110ml$ of suspension, measured initially. The particles are dyed using water-based food coloring in order to enhance their visibility, and are then allowed to dry overnight. The suspensions are prepared by first weighing the two phases separately (ϕ_0 fraction of particles and $1-\phi_0$ fraction of liquid), and then mixing them manually using a stirring rod; the mixing procedure is carried out slowly in order to prevent entrapment of air bubbles. A uniformly mixed suspension is then poured into the reservoir, the gate is raised, and the suspension in allowed to flow down the incline. The suspension remains well-mixed during the short time-interval between pouring into the reservoir and raising the gate. In fact, in all of our experiments, the separation of phases, i.e. settling, would occur only some distance down the incline, depending on the configuration.

The total suspension volume is a key parameter. In a series of validation experiments we observe that during the preparation of each run we consistently lose $\approx 25\%$ of the total measured suspension volume. A significant contribution to this loss is due to suspension remaining in the mixing container after the pouring into the reservoir is carried out; a smaller amount of suspension also remains in the reservoir after the gate release. The volume loss is the largest source of systematic error in the experiments. We take this into account by considering correspondingly reduced suspension volume in the numerical simulations of our model equations.

A large number (>60) of experimental runs have been carried out over a long period of time. With the environment in the lab (air temperature and relative humidity) maintained at a constant level via an air-conditioning unit, we have developed a simple procedure for preparing the solid substrate before each set of experiments, to ensure identical wetting properties and reproducibility of results for all the runs. In addition, we want to minimize the occurrence of the fingering instability, which complicates front tracking and subsequent analysis. The procedure is as follows. The track surface is first cleaned using a dish-washing liquid. This is followed by allowing $110ml$ of clear $1000\,cSt$ PDMS to flow down the incline at $\alpha = 45°$ for 1 hour, leaving behind a thin precursor layer. Without recording any data yet, $110ml$ of $\phi_0 = 0.2$ suspension is then allowed to flow down the incline until it drains into the tank. The left-over particles and liquid are carefully cleaned using a rubber squeegee. The track is now ready for recorded experimental runs. The squeegee is used after every subsequent run. Each run is repeated to confirm the reproducibility of the results. We note that, while this protocol leads to a good reproducibility for the settled regime, this may not be the case when much denser suspensions are used (i.e. the ridged regime).

In this study we are interested in the details of the *settled* regime. We record the separation of the particle and liquid phases and monitor the motion of the two distinct fronts down the incline, with the clear liquid front moving ahead of the particle one. In order to capture the settled regime experimentally, we choose the parameter values based on the extensive experiments carried out in Murisic *et al.* (2011). In particular, we concentrate on small to moderate values of the bulk particle volume fraction and inclination angle: $\phi_0 = 0.2, 0.3, 0.4$ and $\alpha = 5° \dots 40°$ in 5°-increments. The experimental data consists of high-definition videos, captured in a 1920×1080-pixel resolution at $25\,fps$. The videos are recorded using a Canon EOS Rebel T2i digital SLR camera utilizing a Canon EF-S 18-55mm f/3.5-5.6 wide-angle lens. The device is mounted on a tall tripod, so that the camera is $\approx 1m$ above the flow and $\approx 50cm$ below the release gate, while the lens surface is roughly parallel to the track surface. This allows us to capture the whole length of the track with minimal distortion. Each flow is recorded from the time-instant it is released from the reservoir, until the clear liquid front reaches the lower end of the track. In our analysis, we mainly focus on the time-interval starting with the first occurrence

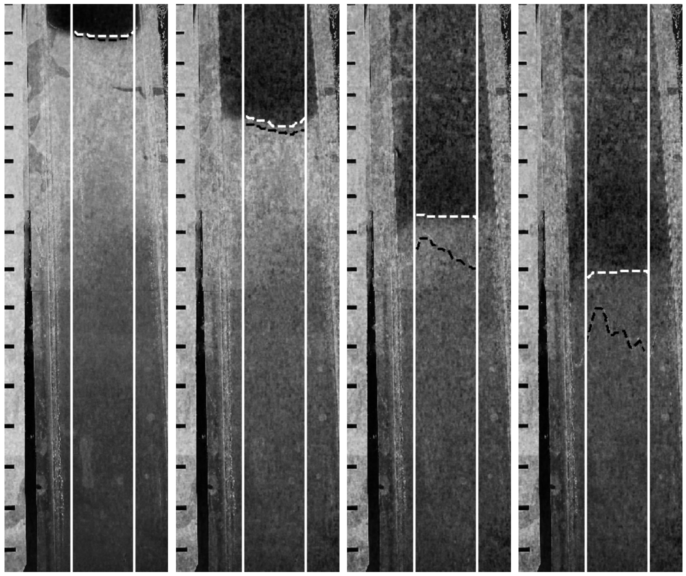

FIGURE 6. The suspension flow with $\phi_0 = 0.3$ and $\alpha = 25^\circ$ at different stages; time increases left to right; the black and white dashed lines show the clear liquid and particle front positions; the black tick-marks on the side of the track are $5cm$ apart; darker regions in the particulate bed indicate higher particle numbers.

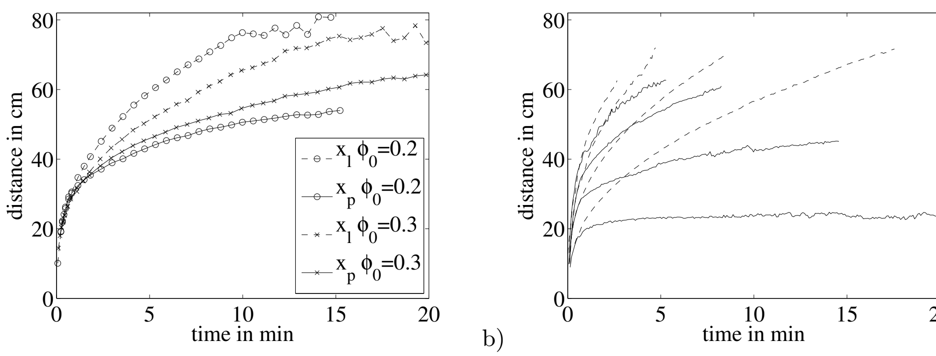

FIGURE 7. Time dependence of the liquid front position, x_ℓ, and the particle front position, x_p, in the experiments with: a) $\phi_0 = (0.2, 0.3)$ and $\alpha = 25^\circ$; and b) $\phi_0 = 0.2$ and $\alpha = (10, 20, 30, 40)^\circ$, where the full lines denote x_p and the dashed ones x_ℓ; larger α values result in steeper curves.

of the two distinct fronts. Typically, this amounts to $12 - 25min$ of evolution, depending on ϕ_0 and α values. The videos are then dissected, extracting individual images at a rate of $0.2\,fps$. The image post-processing is carried out using a specialized code in MATLAB (MathWorks). It identifies the particle and the liquid front in each image, their visibility enhanced by the particle coloring and the brightness variations near the clear liquid contact line. The preparation of the solid substrate also helps as it leads to fairly straight fronts with reduced fingering of the clear liquid front. In each image, the code detects the two curves in the (x, y) plane corresponding to the two fronts. The values x_p and x_ℓ for each image are obtained by averaging along the curves corresponding to particle and liquid fronts respectively; processing a series of images in this manner yields the time-evolution of the front positions, $x_p(t)$ and $x_\ell(t)$. This procedure gives reproducible results within $\pm 5\%$.

A typical evolution is shown in Fig. 6. The qualitative experimental observations are as follows. Initially, a uniform (well-mixed) suspension moves down the incline. Toward the end of this initial transient, denoted by $t \in [0, t_{\text{trans}}]$, a transition occurs, where two distinct fronts form, and the clear liquid front moves ahead of the particle front. We find that the duration of the transient regime increases with α; it also increases with ϕ_0. The separation of phases is detectible once the suspension front has moved $15 - 40cm$ down the incline, depending on the values of α and ϕ_0. Furthermore, for small angles, $\alpha < 10°$, the particle front practically comes to a halt, at least on the timescale of our experiments. The increase in the value of α leads to an increase in the ratio of the front positions toward unity: $x_p(t)/x_\ell(t) \to 1$. Naturally, above a critical value of α, defined by 2.12, the flow undergoes a transition toward the ridged regime, where the particles move to the contact line of the flow; in our experiments, we stay well away from this transition. Figure 7 shows in some detail the dependence of the evolution of x_ℓ and x_p on the values of α and ϕ_0.

We note that t_{trans} turns out be an important parameter in our model, as it effectively determines the time-instant when our equilibrium assumption in the z-direction becomes valid, see §4 below. In our experiments, the unsteadiness of the flow may in fact persist beyond the time-instant when the two distinct fronts are first detected by our apparatus. Hence, we are only able to directly observe a lower bound for t_{trans}.

We proceed by carrying out the numerical simulations of Eqs. 2.11, and comparing the model predictions with the experimental data for different α and ϕ_0 values.

4. Comparison: model predictions vs. experimental data

The governing system in 2.11 is solved numerically next, in order to carry out a quantitative comparison with the experiments. The equilibrium portion, namely the boundary value problem in 2.11f) and g), is solved for intermediate quantities $\tilde{\phi}$ and $\tilde{u}$ using a shooting method with Runge-Kutta; the dynamic transport equations, i.e. 2.11a-d), are solved for the main variables h and n using an upwind scheme. The initial data we use for this purpose is

$$h(0,x) = \begin{cases} h_0 & -d_x < x < 0 \\ 0 & \text{else} \end{cases}, \qquad n(0,x) = \phi_0 h(0,x),$$

representing the well-mixed suspension at $t = 0$, like in the experiments. The average concentration, $0 < \phi_0 < \phi_{\text{m}}$, in the simulations is adjusted to correspond to each particular experiment, and the quantity h_0 is such that the total volume is $V = 0.75 \cdot 110\, ml = h_0\, d_x\, d_y$. As noted earlier, the factor 0.75 accounts for the loss of suspension volume during the preparation of each experiment. Here, the width of the track is $d_y = 14\, cm$, and $d_x = 10\, cm$, the length of the reservoir, is a parameter in the initial data.

We also quantify the transient stage, here denoted by the time-interval $[0, t_{\text{trans}}]$. This transient includes the early well-mixed phase, but it may also extend beyond the time-instant when the two distinct fronts are first detected; in our experiments, the suspension typically travels $15 - 40\, cm$ before the clear liquid front becomes visible. Hence, the experimental observations only yield a lower bound for t_{trans}. An additional issue is the fact that the equilibrium assumption in the z-direction is clearly not valid during the well-mixed stage when only a single front is detectible. Therefore, the governing system in 2.11 is not appropriate for describing the evolution for $0 < t \leq t_{\text{trans}}$. In order to derive a governing system appropriate for this time-interval, we employ the well-mixed assumption, i.e. $\tilde{\phi}(t,x;s) = \tilde{\phi}(t,x) = \phi_0(t,x)$; this is equivalent to considering the

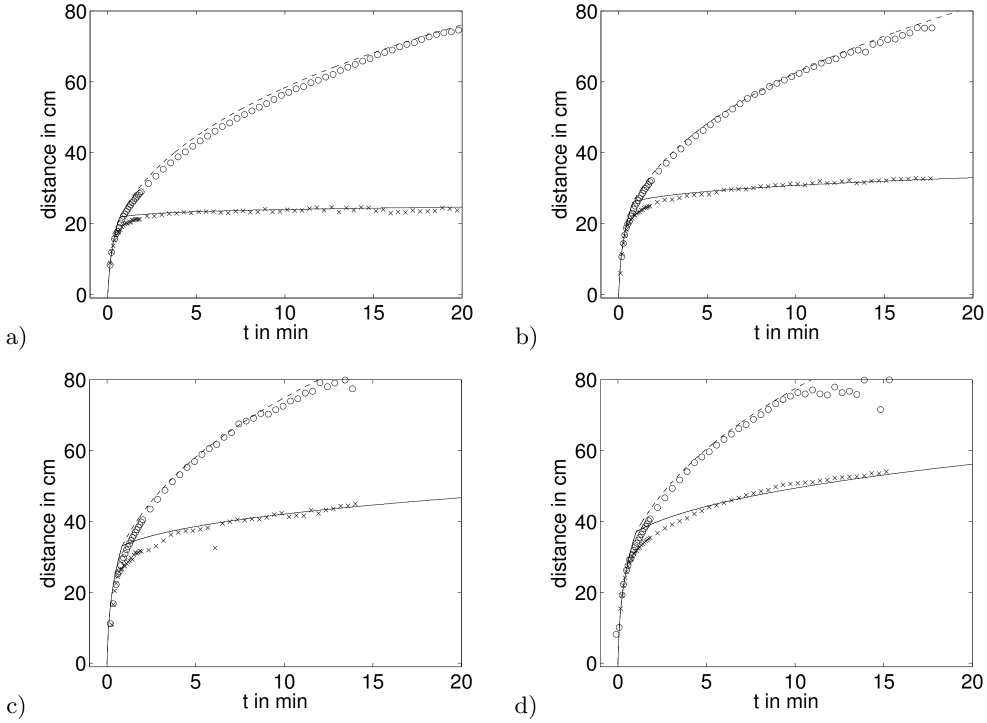

FIGURE 8. Experiment vs Simulation for $\phi_0 = 0.2$ and: a) $\alpha = 10°$; b) $\alpha = 15°$; c) $\alpha = 20°$; and d) $\alpha = 25°$. The dashed line is the liquid front $x_\ell(t)$, whereas the full line shows the particle front $x_p(t)$.

colloidal limit, $\eta \to 0$. The resulting advection equations for h and n are

$$\partial_t h + \partial_x \tilde{F} = 0, \qquad \partial_t n + \partial_x\big(\phi_0 \tilde{F}\big) = 0, \tag{4.1}$$

with $\tilde{F} = (1 + \phi_0 \rho_s) h^3 / \big(3\bar{\nu}\big)$ and $\bar{\nu} = (1 - \phi_0/\phi_{\mathrm{m}})^{-2}$. We note that n is advected trivially, and is given by $n(t,x) = \phi_0(t,x) h(t,x)$. Hence, in order to account for the transient stage, we solve Eqs. 4.1 for $0 < t \le t_{\mathrm{trans}}$, while the system 2.11 is solved for later times, $t > t_{\mathrm{trans}}$.

Figure 8 shows a comparison between the model predictions and the experimental data for a fixed average concentration $\phi_0 = 0.2$, and a few different values of the inclination angle, $\alpha = (10, 15, 20, 25)°$. The agreement is good, both in the transient stage and for later times, when the equilibrium assumption is valid. We notice, that during the transient stage, the colloid approximation leads to a slight overestimation of the mobility of the fronts, particularly the particle one. The comparison is carried out for $t < 20min$ only, due to the influence of the transient in the simulations: the overestimation of $x_\ell(t)$ and $x_p(t)$ for $0 < t \le t_{\mathrm{trans}}$ hinders the model prediction for long-time behavior of the two fronts. Hence, further analysis of the transient stage and more precise measurements of t_{trans} are required in order to accurately predict the motion of the fronts for longer time-intervals. Figures 9 and 10 show equivalent results for $\phi_0 = 0.3$ and $\phi_0 = 0.4$, and various values of α; they both indicate similar degree of agreement between theory and experiments compared to the $\phi_0 = 0.2$ case. We note that only small values of α are used with $\phi_0 = 0.4$, as larger values result in ridged regime. Figure 10 indicates that the model's overestimation of the mobility of the fronts during the transient phase is

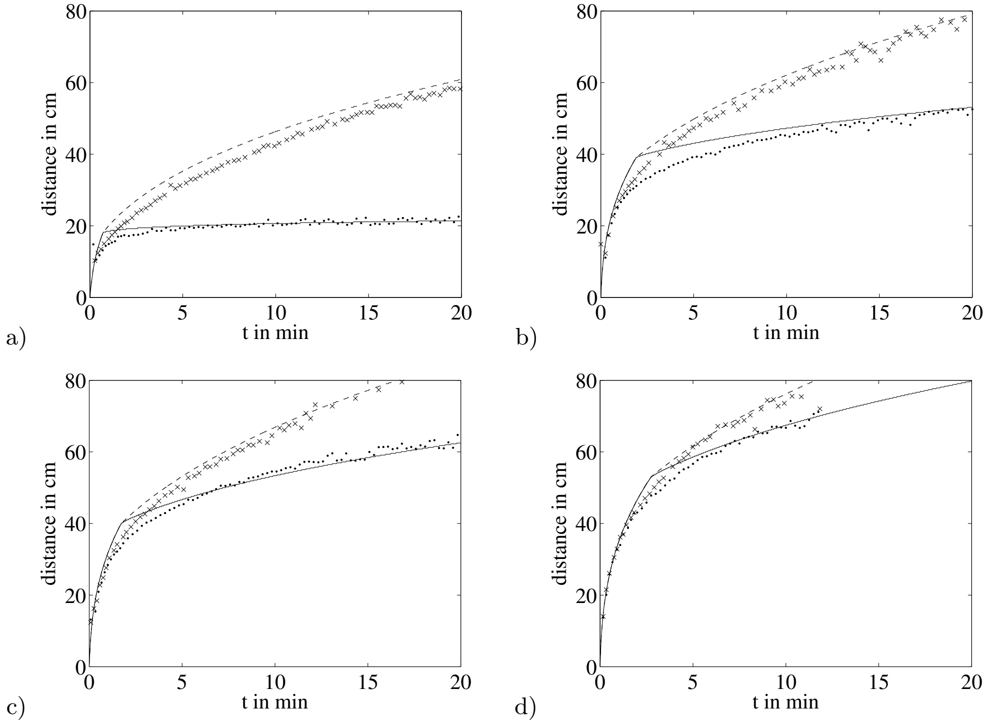

FIGURE 9. Experiment vs Simulation for $\phi_0 = 0.3$ and: a) $\alpha = 10°$; b) $\alpha = 20°$; c) $\alpha = 25°$; and d) $\alpha = 30°$. The dashed line is the liquid front $x_\ell(t)$, whereas the full line shows the particle front $x_p(t)$.

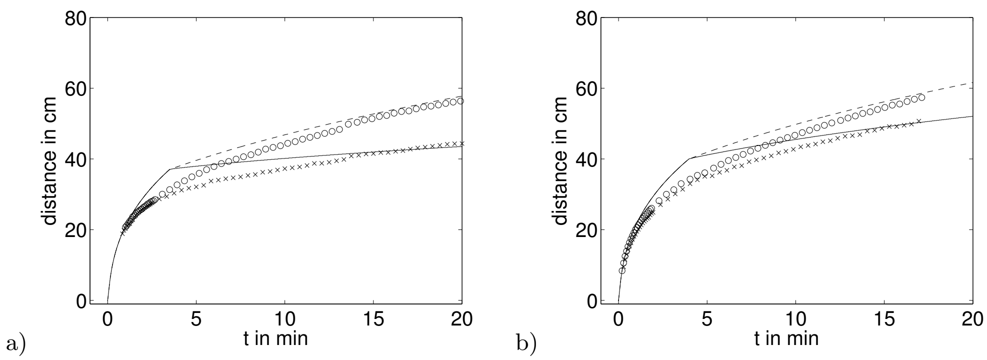

FIGURE 10. Experiment vs Simulation for $\phi_0 = 0.4$ and: a) $\alpha = 15°$; and b) $\alpha = 20°$. The dashed line is the liquid front $x_\ell(t)$, whereas the full line shows the particle front $x_p(t)$.

particularly pronounced for $\phi_0 = 0.4$. Other factors may also affect the model prediction for denser suspensions, see discussion below.

5. Conclusions

In this paper, we focus on the *settled* regime observed in particle-laden thin-film flows on an incline. In this regime, particles settle to the solid substrate and the clear liquid film flows over the sediment. Two distinct fronts form: the slower particle and the faster clear liquid one.

We first derive a continuum model, starting from the Stokes' equations for the suspension and a transport equation for the particles. The particle model is a diffusive one, including the effects of shear-induced migration and hindered settling due to gravity. We apply the lubrication-style scales and carry out an asymptotic analysis of the resulting equations. Our main assumption is that the particle distribution in the z-direction is in equilibrium, i.e. that the corresponding dynamics occurs on a rapid time-scale so that the steady-state is quickly established and the total particle flux in the z-direction is zero. Hence, we are able to reconstruct the z-profiles for the particle volume fraction and the suspension velocity. Our asymptotics approach then allows us to connect the leading order equilibrium model to the slow dynamics of particle and suspension transport down the incline, in the x-direction. We switch to the averaged quantities, the film thickness and the particle number, which obey a coupled system of advection equations (a pair of hyperbolic conservation laws), thereby closing the approximation and completing the theoretical framework. We proceed by confirming the hyperbolicity of the transport equations, and analyzing the dilute limit for which we derive an analytic solution, and study the behavior of the particle and the clear liquid fronts in the finite volume case as $t \to \infty$.

Next, we carry out experiments using finite fixed volume suspensions, consisting of glass beads and PDMS. In the experiments, we vary the bulk particle volume fraction and the inclination angle of the solid substrate within the permitted range for the settled regime. Our experimental setup allows us to detect the particle and the clear liquid fronts, and precisely monitor their motion down the incline. We also detect a short initial transient phase, in which the mixture remains well-mixed, and identify the loss of volume in the experiment preparation as the single largest source of systematic error.

Finally, we compute the numerical solutions of our governing system of equations, and compare the model predictions for the case of finite suspension volume with the experimental data. To take into account the transient phase observed in the experiments, the colloidal limit for our model is also considered: we use the colloidal model to capture the transient stage, and then switch to the full model for later times. The result is a good agreement between the theory and the experiments, especially for lower values of average particle volume fraction, ϕ_0. For larger values of this parameter, the influence of the transient regime becomes more significant.

In order to improve our model, a detailed investigation of the transient phase is required, including both careful experiments and a theoretical approach. In particular, an important question is how early the equilibrium in the z-direction may be assumed. This involves more precise experimental measurements of the transient time t_{trans}. Another interesting questions is the validity of the hinderance model and the Krieger-Dougherty $\mu(\phi)$ relation for denser suspensions. Future work should also include higher order terms in the dynamic equations, e.g. the terms corresponding to the capillary and normal gravitational forces. This would allow for a comprehensive study of the different settling regimes, the evolution of the contact line region, and the details of the fingering instability occurring in these flows.

Acknowledgement

This work was supported by NSF grant DMS-1048840 and UC Lab Fees Research Grant 09-LR-04-116741-BERA.

REFERENCES

Acrivos, A., Batchelor, G.K., Hinch, E.J., Koch, D.L. & Mauri, R. 1992 Longitudinal shear-induced diffusion of spheres in a dilute suspension. *Journal of Fluid Mechanics* **240**, 651.

Batchelor, G. K. 1972 Sedimentation in a dilute suspension of spheres. *J.Fluid Mech.* **52**, 245.

Brady, J. F. 1993 The rheological behavior of concentrated colloidal dispersions. *J.Chem. Phys.* **99**, 567.

Brady, J. F. & Morris, J. F. 1997 Microstructure of strongly sheared suspensions and its impact on rheology and diffusion. *J.Fluid Mech.* **348**, 103.

Cook, B. P. 2008 Theory for particle settling and shear-induced migration in thin-film liquid flow. *Phys. Rev. E* **78**, 045303.

Cook, B. P., Bertozzi, A. L. & Hosoi, A. E. 2007 Shock solutions for particle-laden thin films. *SIAM J.Appl. Math.* **68**, 760.

Davis, R. H. & Acrivos, A. 1985 Sedimentation of noncolloidal particles at low Reynolds-numbers. *Ann. Rev. Fluid Mech.* **17**, 91.

Glowinski, R., Pan, T.W., Hesla, T.I., Joseph, D.D. & Periaux, J. 2001 A fictitious domain approach to the direct numerical simulation of incompressible viscous flow past moving rigid bodies: application to particulate flow. *Journal of Computational Physics* **169** (2), 363.

Grunewald, N., Levy, R., Mata, M., Ward, T. & Bertozzi, A.L. 2010 Self-similarity in particle-laden flows at constant volume. *Journal of Engineering Mathematics* **66** (1), 53.

Huppert, H. 1982 Flow and instability of a viscous current down a slope. *Nature* **300**, 427.

Kondic, L. 2003 Instability in the gravity driven flow of thin liquid films. *SIAM Review* **45**, 95.

Kondic, L. & Bertozzi, A. L. 1999 Nonlinear dynamics and transient growth of driven contact lines. *Phys. Fluids* **11**, 3560.

Kynch, G.J. 1952 A theory of sedimentation. *Transactions of the Faraday society* **48**, 166.

Leighton, D. & Acrivos, A. 1987*a* Measurement of shear-induced self-diffusion in concentrated suspensions of spheres. *J.Fluid Mech.* **177**, 109.

Leighton, D. & Acrivos, A. 1987*b* The shear-induced migration of particles in concentrated suspensions. *J.Fluid Mech.* **181**, 415.

Murisic, N., Ho, J., Hu, V., Latterman, P., Koch, T., Lin, K., Mata, M. & Bertozzi, A.L. 2011 Particle-laden viscous thin-film flows on an incline: Experiments compared with a theory based on shear-induced migration and particle settling. *Physica D: Nonlinear Phenomena* **240**, 1661.

Nott, P. R. & Brady, J. F. 1994 Pressure-driven flow of suspensions - simulation and theory. *J.Fluid Mech.* **275**, 157.

Phillips, R. J., Armstrong, R. C., Brown, R. A., Graham, A. L. & Abbott, J. R. 1992 A constitutive equation for concentrated suspensions that accounts for shear-induced particle migration. *Phys. Fluids A* **4**, 30.

Richardson, J. F. & Zaki, W. N. 1954 The sedimentation of a suspension of uniform spheres under conditions of viscous flow. *Chem. Eng. Sci.* **3**, 65.

Schaflinger, U., Acrivos, A. & Zhang, K. 1990 Viscous resuspension of a sediment within a laminar and stratified flow. *Int. J.Multiphase Flow* **16**, 567.

Song, C., Wang, P. & Makse, H.A. 2008 A phase diagram for jammed matter. *Nature* **453** (7195).

Timberlake, B. D. & Morris, J. F. 2005 Particle migration and free-surface topography in inclined plane flow of a suspension. *J.Fluid Mech.* **538**, 309.

Van Der Werff, J. C. & De Kruif, C. G. 1989 Hard-sphere colloidal dispersions: The scaling of rheological properties with particle size, volume fraction, and shear rate. *J. Rheol.* **33** (3).

Ward, T., Wey, C., Glidden, R., Hosoi, A. E. & Bertozzi, A. L. 2009 Experimental study of gravitation effects in the flow of a particle-laden thin film on an inclined plane. *Phys. Fluids* **21**, 083305.

Zhou, J. J., Dupuy, B., Bertozzi, A. L. & Hosoi, A. E. 2005 Theory for shock dynamics in particle-laden thin films. *Phys. Rev. Lett.* **94**, 117803.